J|A|C|S
ARTICLES
Published on Web 04/03/2004

Molecular Control of Recombination Dynamics in Dye-Sensitized Nanocrystalline TiO_2 Films: Free Energy vs Distance Dependence

John N. Clifford,[†] Emilio Palomares,[†] Md. K. Nazeeruddin,[‡] M. Grätzel,[‡] Jenny Nelson,[§] X. Li,[†] Nicholas J. Long,[†] and James R. Durrant*,[†]

Contribution from the Centre for Electronic Materials and Device, Departments of Chemistry and Physics, Imperial College London, Exhibition Road, SW7 2AZ, London, U.K., and Laboratory for Photonics and Interfaces, Institute of Physical Chemistry, Swiss Federal Institute of Technology, CH-1015 Lausane, Switzerland

Received December 3, 2003; E-mail: j.durrant@imperial.ac.uk

Abstract: In this paper we address the dependence of the charge recombination dynamics in dye-sensitized, nanocrystalline TiO_2 films upon the properties of the sensitizer dye employed. In particular we focus upon dependence of the charge recombination kinetics upon the dye oxidation potential $E^0(D^+/D)$, determined electrochemically, and the spatial separation r of the dye cation HOMO orbital from the metal oxide surface, determined by semiempirical calculations. Our studies employed a series of ruthenium bipyridyl dyes in addition to porphyrin and phthalocyanine dyes. A strong correlation is observed between the recombination dynamics and the spatial separation r, with variation in r by 3 Å resulting in a more than 10-fold change in the recombination half-time $t_{50\%}$. This correlation is found to be in agreement with electron tunneling theory, $t_{50\%} \propto \exp(-\beta r)$ with $\beta = 0.95 \pm 0.2$ Å^{-1}. In contrast, the recombination dynamics were found to be relatively insensitive to variations in $E^0(D^+/D)$, indicative of the recombination reaction lying near the peak of the Marcus free energy curve, $\Delta G \sim \lambda$, and with $\lambda \sim 0.8$ eV. A correlation is also observed between the recombination half-time and the temporal shape of the kinetics, with faster recombination dynamics being more dispersive (less monoexponential). Comparison with numerical Monte Carlo type simulations suggests this correlation is attributed to a shift from fast recombination dynamics primarily limited by dispersive electron transport within the metal oxide film to slower dynamics primarily limited by the interfacial electron-transfer reaction. We conclude that the primary factor controlling the charge recombination dynamics in dye-sensitized, nanocrystalline TiO_2 films is the spatial separation of the dye cation from the electrode surface. In particular, we show that for the $Ru(dcbpy)_2NCS_2$ dye series, the use of X = NCS rather than X = CN results in a 2 Å shift in the dye cation HOMO orbital away from the electrode surface, causing a 7-fold retardation of the recombination dynamics, resulting in the remarkably slow recombination dynamics observed for this sensitizer dye.

Introduction

Supramolecular electron-transfer complexes have received extensive attention over the past 15 years.[1−4] Such studies have addressed the correlation between the structure and redox properties of such complexes and the electron-transfer dynamics observed following optical excitation. These dynamics have been shown to be in good agreement with nonadiabatic electron-transfer theory.[5] Attention is now increasingly focusing on heterogeneous electron-transfer complexes, involving interfacial electron-transfer processes between molecular redox species and inorganic nanoparticles or electrode surfaces.[6−8] A system of particular interest is dye-sensitized, nanocrystalline metal oxide electrodes, of importance due to their technological applications in for example dye-sensitized solar cells and electrochromic windows.[9−11] The high surface and optical transparency of these electrodes make them ideally suited to spectroscopic studies of interfacial electron-transfer dynamics. Moreover the theoretical framework for such interfacial electron-transfer dynamics was

[†] Centre for Electronic Materials and Device, Department of Chemistry, Imperial College London.
[‡] Swiss Federal Institute of Technology.
[§] Department of Physics, Imperial College London.

(1) Argazzi, R.; Bignozzi, C. A.; Heimer, T. A.; Meyer, G. J. *Inorg. Chem.* **1997**, *36*, 2−3.
(2) Gray, H. B.; Winkler, J.; Balzani, V. In *Electron Transfer in Chemistry*; Wiley-VCH: Weinheim, Germany, 2001; Vol. 3.
(3) Petersen, J. D.; Morgan, L. W.; Hsu, L.; Billadeau, M. A.; Ronco, S. E. *Coord. Chem. Rev.* **1991**, *111*, 319−324.
(4) El-Khouly, M. E.; Rogers, L. M.; Zandler, M. E.; Suresh, G.; Fuitsuka, M.; Ito, O.; D′Souza, F. *ChemPhysChem* **2003**, *4*, 474−481.
(5) Moser, C. C.; Keske, J. M.; Warncke, K.; Farid, R. S.; Dutton, P. L. *Nature* **1992**, *355*, 796−802.
(6) Bignozzi, C. A.; Argazzi, R.; Kleverlaan, C. J. *Chem. Soc. Rev.* **2000**, *29*, 87−96.
(7) Connolly, S.; Nagaraja, S. R.; Rizza, R.; Zaccheroni, N.; Fitzmaurice, D. *Coord. Chem. Rev.* **1999**, *185−186*, 277−295.
(8) Marguerettaz, X.; Fitzmaurice, D. *J. Mater. Chem.* **1998**, *8*, 2157−2164.
(9) Garcia, C. G.; de Lima, J. F.; Murakami Iha, N. Y. *Coord. Chem. Rev.* **2000**, *196*, 219−247.
(10) Jana, A. K. *J. Photochem. Photobiol., A* **2000**, *132*, 1−17.
(11) Kalyanasundaram, K.; Gratzel, M. *Coord. Chem. Rev.* **1998**, *77*, 347−414.

established by Gerischer and co-workers in the 1960s.[12−14] However, the practical application of this theory to dye-sensitized, nanocrystalline metal oxide electrodes remains to date relatively limited.

In this paper we are concerned with influence of the molecular sensitizer dye design upon the interfacial electron-transfer dynamics of dye-sensitized nanocrystalline TiO_2 films. The design of new sensitizers which combine strong visible light absorption with favorable electron-transfer dynamics is a key issue in the development and optimization of dye-sensitized solar cells.[15−17] The charge separation process in such dye-sensitized films is based upon electron injection from the excited state of the dye into the conduction band of TiO_2. We focus here upon the charge recombination reaction between photoinjected electrons and the dye cations, which follows this light-driven charge separation. This recombination reaction is of particular interest due its potential importance in limiting the performance of dye-sensitized photoelectrochemical solar cells.

Following nonadiabatic electron-transfer theory,[12−14] the rate of electron transfer between donor and acceptor states is given by

$$k_{et} = \frac{{H_{AB}}^2}{\sqrt{4\pi\lambda k_B T}} \exp\left(-\frac{(\Delta G^0 - \lambda)^2}{4\lambda k_B T}\right) \quad (1)$$

where H_{AB}^2 is the electronic coupling between the donor and acceptor states, ΔG^0 is the reaction free energy, and λ is the reorganization energy. For reactions involving molecular species absorbed at electrode surfaces, it is necessary to integrate eq 1 over all possible donor or acceptor states of the electrode, as has been discussed previously.[18] It is apparent from eq 1 that molecular design may be employed to modulate the electron-transfer dynamics by varying the following parameters: the electron coupling (H_{AB}^2), the reaction free energy (ΔG^0), and the reorganization energy (λ). Of these three parameters, the reorganizational energy is largely controlled by the polarity of the surrounding solvent and is therefore less amenable to control by design of the redox molecule. The term H_{AB}^2 corresponds to electron tunneling through a potential barrier and therefore shows an exponential dependence upon spatial separation r of the donor and acceptor states:

$$H_{AB}^2 = H_0^2 e^{-\beta r} \quad (2)$$

where β is a function of the barrier height of the intervening media and is again less amenable to molecular control. It can be concluded that the two key parameters which can be varied by molecular design to modulate the interfacial electron-transfer dynamics are the r and ΔG^0. For charge recombination in dye-sensitized electrodes, r effectively corresponds to the spatial separation of the dye cation HOMO orbital from the electrode surface, while ΔG^0 corresponds to the difference in free energy between the dye oxidation midpoint potential $E^0(D^+/D)$ and the electrode Fermi level E_F.

The experimental strategy employed in this study is based upon employing transient absorption spectroscopy to interrogate the interfacial recombination dynamics in dye-sensitized, nanocrystalline TiO_2 films as a function of the sensitizer dye employed. The primary objective of our study is to elucidate the relative importance of distance r and free energy ΔG^0 in controlling these interfacial recombination dynamics. The dependence of this recombination reaction upon both of these parameters has been addressed in several previous studies.[19−24] Such studies have typically reported a significant dependence of the recombination kinetics upon dye oxidation potential ($E^0(D^+/D)$) and therefore upon ΔG^0. Experimental fits of such dependencies to eq 1 have yielded estimates for the reorganizational energy for the recombination reaction of 1−1.4 eV, with most experimental data lying in the Marcus "inverted region".[20,22] This inverted-region behavior, resulting in a retardation of the recombination dynamics, has been suggested to be important in minimizing recombination losses in dye-sensitized solar cells.[25] In contrast studies of the distance dependence have, to date, been more limited and less conclusive. In general, studies employing smaller, more tightly bound sensitizer dyes exhibit faster recombination kinetics, while larger dyes, where the dye cation can be expected to lie further from the electrode surface, exhibit slower kinetics. We have recently reported two studies where a change of the design of the molecular dye has been shown to result in significant retardation of the recombination dynamics; in both cases this retardation was attributed to an increase of separation of the dye cation from the TiO_2 surface.[19,26] In contrast, in a study employing a tripodal dye-binding motif as a "molecular bridge" to control the orientation of the sensitizer dye relative to the electrode surface, the recombination dynamics were found to be independent of the spatial separation of the sensitiser dye from the electrode surface.[24]

The recombination reaction can most simply be expected to exhibit second-order kinetics (first order in both electron and dye cation concentrations) and has indeed been analyzed as such.[20] Our own studies have however focused more on the influence of the electron-transport dynamics within the metal oxide film on the recombination dynamics.[27,28] We have demonstrated that the temporal form of the recombination dynamics, and their dependence upon the bias applied to the metal oxide electrode, can be successfully simulated by a model based upon electron transport through an energetic distribution of trap sites within the TiO_2 particles.[27] More recently, we have demonstrated, by employing two different sensitizer dyes, that it is possible to move between regimes of transport-limited and

(12) Gerischer, H.; Michel-Beyerle, M. E.; Rebentrost, F.; Tributsch, H. *Electrochim. Acta* **1968**, *13*, 1509−1515.
(13) Gerischer, H. *Z. Phys. Chem.* **1960**, *26*, 223−247.
(14) Gerischer, H. *Adv. Electrochem. Electrochem. Eng.* **1961**, *1*, 139−232.
(15) O'Regan, B.; Gratzel, M. *Nature* **1991**, *353*, 737.
(16) Zakeeruddin, S. M.; Nazeeruddin, M. K.; Humphry-Baker, R.; Pechy, P.; Quagliotto, P.; Barolo, C.; Viscardi, G.; Gratzel, M. *Langmuir* **2002**, *18*, 952−954.
(17) Argazzi, R.; Bignozzi, C. A.; Heimer, T. A.; Castellano, F. N.; Meyer, G. J. *Inorg. Chem.* **1994**, *33*, 5741−5749.
(18) Schmickler, W. *Interfacial Electrochemistry*; Oxford University Press: Oxford, U.K., 1996.
(19) Clifford, J. N.; Yahioglu, G.; Milgrom, L. R.; Durrant, J. R. *Chem. Commun.* **2002**, *12*, 1260−1261.
(20) Kuciauskas, D.; Freund, M. S.; Gray, H. B.; Winkler, J. R.; Lewis, N. S. *J. Phys. Chem. B* **2001**, *105*, 392−403.
(21) Yan, S. G.; Prieskorn, J. S.; Kim, Y.; Hupp, J. T. *J. Phys. Chem. B* **2000**, *104*, 10871−10877.
(22) Ramakrishna, G.; Ghosh, H. N. *J. Phys. Chem. B* **2001**, *105*, 7000−7008.
(23) Gaal, D. A.; Hupp, J. T. *J. Am. Chem. Soc.* **2000**, *122*, 10956−10963.
(24) Galoppini, E.; Guo, W.; Zhang, W.; Hoertz, P. G.; Qu, P.; Meyer, G. J. *J. Am. Chem. Soc.* **2002**, *124*, 7801−7811.
(25) Hagfeldt, A.; Gratzel, M. *Chem. Rev.* **1995**, *95*, 49−68.
(26) Hirata, N.; Lagref, J.-J.; Palomares, E. J.; Durrant, J. R.; Nazeeruddin, M. K.; Gratzel, M.; Di Censo, D. *Chem.−Eur. J.* **2004**, *10*, 525−600.
(27) Nelson, J.; Haque, S. A.; Klug, D. R.; Durrant, J. R. *Phys. Rev. B* **2001**, *63*, 5321−5329.
(28) Nelson, J. *J. Phys. Rev.* **1999**, *59*, 15374.

Scheme 1. Schematic Representation of Electron-Transfer Dynamics for Dye-Sensitized, Nanocrystalline TiO_2[a]

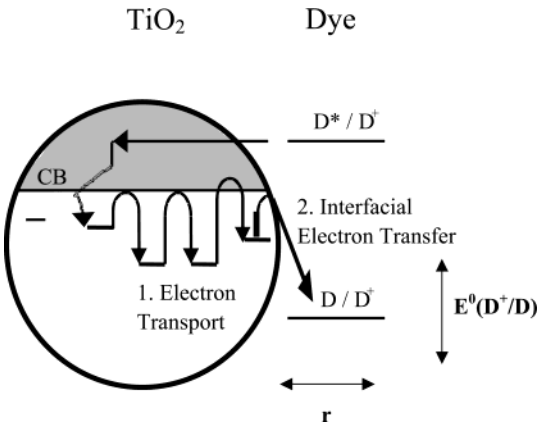

[a] This scheme illustrates how the charge recombination reaction observed following photoinduced electron injection may be rate-limited by either electron transport dynamics within the TiO_2 nanoparticles or by the electron-transfer rate constant at the dye/metal oxide interface. In this paper we are concerned with the dynamics of charge recombination as a function of dye oxidation potential $E^0(D^+/D)$ and the spatial separation r of the dye cation from the metal oxide surface.

interfacial electron-transfer-limited recombination,[19] as illustrated in Scheme 1. In this paper we extend the studies to a range of different sensitizer dyes in order to address separately the importance of free energy and distance in controlling the recombination dynamics and discuss the implications of these studies for the optimization of dye sensitized photoelectrochemical solar cells.

Materials and Methods

The structures of the sensitizer dyes employed in this study are shown in Chart 1. The synthetic procedure to obtain the polypyridyl dyes **1-4** has been published previously.[29,30] Porphyrin complexes **5-8** were purchased from Porphyrin Products Inc. and used as received. Phthalocyanine (**9**) was synthesized by methods analogous to those described by Long et al.[31]

Nanocrystalline TiO_2 films were fabricated as detailed elsewhere on conducting glass slides.[32] The resulting films comprised 10−15 nm diameter anatase TiO_2 particles. The film thickness was 4 μm, with a surface area determined by BET analysis of 94 m^2/g. Sensitization of TiO_2 films with dyes **1**−**7** was achieved by immersing the electrodes in 1 mM solutions of these dyes in ethanolic solvents overnight, followed by rinsing in ethanol to remove unadsorbed dye. TiO_2 films were also sensitized with dye **8** in 1 mM solutions, but in dimethylformamide. This dye is prone to aggregate on the surface of TiO_2 over time, so immediately after the correct optical density is obtained, the transient kinetics was recorded. No coadsorbants were used to minimize aggregation, such as 4-*tert*-butylpyridine, as these were found to slow the lifetimes of the charge recombination reaction. All samples were stored, and experiments conducted, at room temperature. Following sensitization, films were covered with a 1:1 ethylene carbonate: propylene carbonate solution and glass cover slide. UV/vis absorption spectra were measured using a Shimadzu 1601 UV−vis spectrometer.

Nanosecond−Millisecond Laser Transmittance Spectroscopy. Transient absorption experiments were conducted using the apparatus reported previously.[33] Samples were excited at 610 nm for all dyes except **5** and **6** (595 nm) and dye **3** (520 nm), employing excitation densities of 20 μJ cm^{-2} (0.8 Hz repetition rate; <1 ns pulse duration), thereby ensuring similar densities of absorbed photons per nanoparticle for all dyes (~0.5 absorbed photons per TiO_2 nanoparticle per laser pulse). The resulting photoinduced changes in optical density were monitored by employing a 100 W Tungsten lamp, with 20 nm bandwidth monochromators before and after sampling, a home-built photodiode-based detection system, and a TDS-220 Tecktronic DSO oscilloscope. Optical absorption measurements performed before and after each transient experiment indicated negligible desorption/degradation of the sensitizer dyes during any of the transient absorption experiments. Experiments were conducted without added redox couple and without externally applied bias.

Electrochemistry. The ground-state oxidation ($E^0(D^+/D)$) values for dyes **1-7** were obtained from previously published electrochemical data.[30,31,34,35] The E^0 value for dye **8** was determined by cyclic voltammetry. The electrolyte used was 0.1 M tetrabutylammonium perchlorate in dimethylformamide (DMF). The working and counter electrodes consisted of platinum wire, and the reference electrode used was Ag/AgCl based (converted to SCE for the purposes of this paper). The scan rate employed was 10 mV s^{-1}, and the voltammetry displayed fully reversible behavior.

ZINDO Calculations. ZINDO calculations were performed on polypyridyl dyes **1**−**4** using HyperChem 7 run on a PC AMD Athlon XP 2000+ 1.25 GHz. The calculations were implemented using the default parameters in the program with the exception that the charge on each complex was altered from 0 to +1 in order to examine the HOMO orbitals of the cation of each complex. The overlap-weighting factors $\sigma\angle\sigma$ and $\pi\angle\pi$ were set at 1.265 and 0.585, respectively, following previous papers in the literature.[34]

Charge Recombination Model Calculations. Numerical simulations of the recombination dynamics followed the continuous-time random walk (CTRW) model as applied previously to dye-sensitized, nanocrystalline TiO_2 films.[27,28] In this Monte Carlo model, electrons (which may be optically or electrically injected) perform a continuous-time random walk on an energetically disordered lattice, characterized by an exponential distribution of site energies, E, of the form $g(E) = N/kT_0 \exp(-(E_{cb} - E)/k_BT_0)$, where N is the density of sites, E_{cb} represents the conduction band edge, and T_0 is the characteristic temperature of the distribution, with $T_0 = T/\gamma$. Electrons move from site to site by thermal activation via the conduction band, as illustrated in Scheme 1. To simulate the transient absorption experiment, equal numbers of dye cations and electrons (n_in_j) are introduced to the lattice at time $t = 0$ to represent cation−electron pairs generated by the laser pulse. These photoinjected electrons diffuse, together with a population n_d of conduction electrons already present in the dark. Charge recombination occurs as soon as an electron reaches a site occupied by a dye cation. Physically this "reactive site" may represent the site on the metal oxide lattice that is closest to the adsorbed dye cation, and the prompt recombination represents a much faster rate for electron transfer to the dye cation than to any neighboring lattice site. Thus the recombination process is *diffusion-limited*. For an excess of electrons relative to dye cations ($n_d \geq n_in_j$), the dye cation population evolves such as a stretched exponential $D(t) = D(0) \exp(-(t/t_0)^\alpha)$. To allow for variation in the rate of electron transfer to the dye cation (see Scheme 1), we introduce a fractional probability, P_{et}, for recombination once an electron reaches a reactive site. This represents a first-order recombination process of rate $k_{et} = \nu P_{et}$ which competes with electron release from the site of

(29) Zakeeruddin, S. M.; Nazeeruddin, M. K.; Humphry-Baker, R.; Gratzel, M.; Shklover, V. *Inorg. Chem.* **1998**, *36*, 5937−5946.
(30) Nazeeruddin, M. K.; Kay, A.; Rodicio, I.; Humphry-Baker, R.; Mueller, E.; Liska, P.; Vlachopolus, N.; Gratzel, M. *J. Am. Chem. Soc.* **1993**, *115*, 6382−6390.
(31) Li, X.; Long, N. J.; Clifford, J. N.; Campbell, C. J.; Durrant, J. R. *New. J. Chem.* **2002**, *26*, 1076−1080.
(32) Palomares, E. J.; Clifford, J. N.; Haque, S. A.; Lutz, T.; Durrant, J. R. *J. Am. Chem. Soc.* **2003**, *125*, 475−482.
(33) Haque, S. A.; Tachibana, Y.; Willis, R. L.; Moer, J. E.; Gratzel, M.; Klug, D. R.; Durrant, J. R. *J. Phys. Chem. B* **2000**, *104*, 538.
(34) Nazeeruddin, M. K.; Zakeeruddin, S. M.; Humphry-Baker, R.; Gorelesky, S. I.; Lever, A. B. P. *Coord. Chem. Rev.* **2000**, *208*, 213−225.
(35) Dolphin, D. *The Porphyrins*; Academic Press: London, 1978; Vol. IV.

Chart 1. Structures of Dyes Employed in the Present Paper, Where **1** Corresponds to $Ru(dcbpy)_2Cl_2$, **2** to $Ru(dcbpy)_2DTC$, **3** to $Ru(dcbpy)_2(CN)_2$, **4** to $Ru(dcbpy)_2(NCS)_2$, **5** to Zinc−*meso*-Porphyrin IX, **6** to Zinc−Coproporphyrin 1, **7** to H_2TCPP, and **8** to $ZnPc(CH_2COOH)_4$

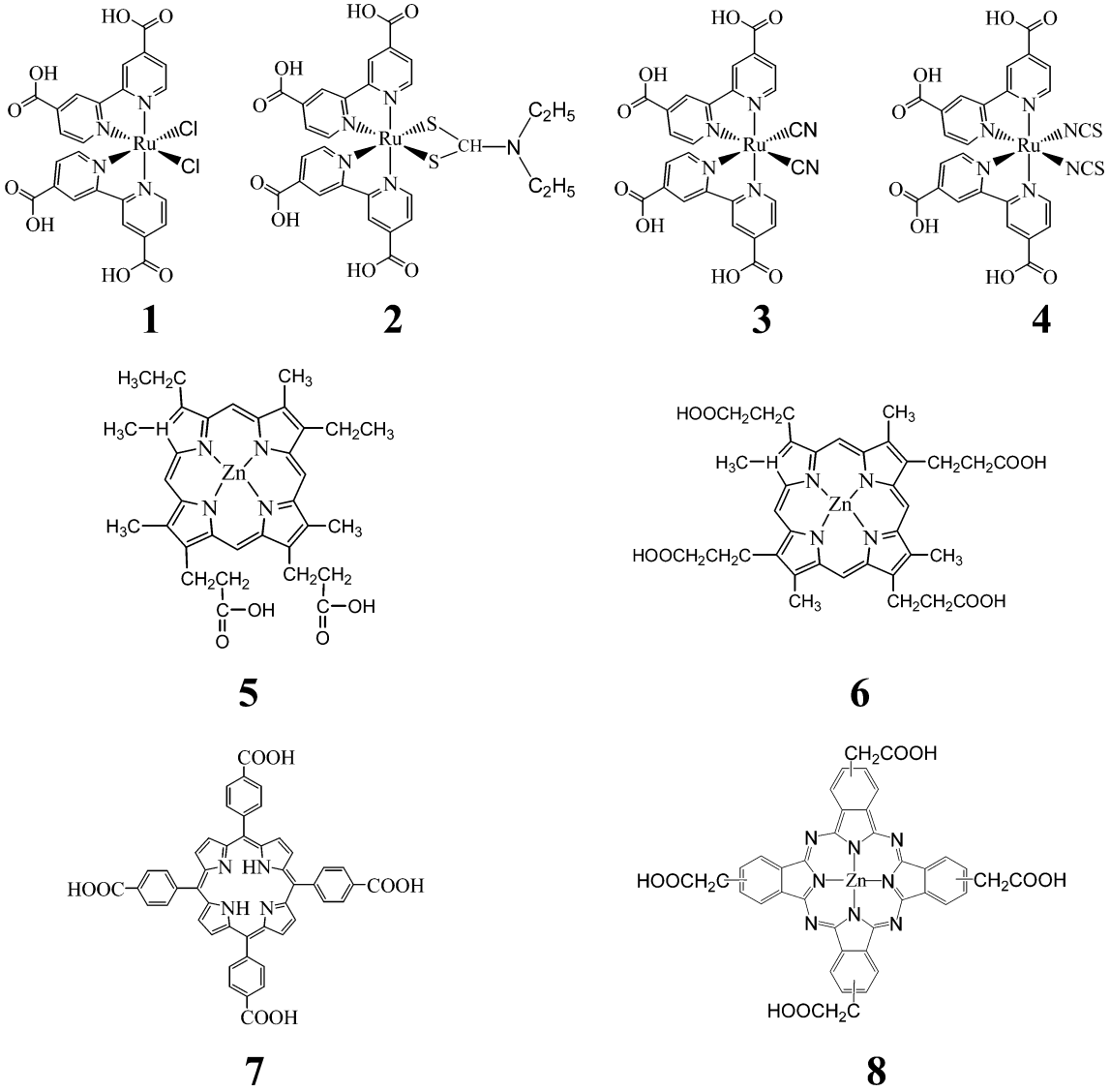

rate ν, where ν is the attempt-to-jump frequency. If recombination does not occur, the electron continues its random walk and the simulation continues. In the limit of fast electron transfer ($P_{et} = 1$), the recombination process is again diffusion-limited and the stretch parameter α is equal to the trap density of states parameter γ, $\alpha = \gamma$, resulting in dispersive (non-monoexponential) dynamics. As P_{et} is reduced, the recombination rate increases and the kinetics becomes less dispersive. The recombination time, as defined from the dye cation half-life $t_{50\%}$, increases slightly superlinearly with P_{et}^{-1} because of the changing shape (α) of the kinetic curve. In the limit where P_{et} tends to 0 (slow electron transfer), the recombination becomes reaction-limited and the recombination rate tends to P_{et}/τ, where τ is the average time to visit all sites on the system and is a function of the system size and the depth of the density of states. In this limit the kinetics are monoexponential, as observed in our previous studies.[19,26]

Results

In all cases, UV−visible absorption spectra of the dye-sensitized TiO_2 films exhibited dye absorption maxima indistinguishable from those observed in solution, indicating minimal dye aggregation and, as expected, relatively weak electronic coupling to the TiO_2 surface. Dye oxidation potentials, determined from solution-phase electrochemistry, are shown in Table 1. It is apparent that ground-state oxidation potentials $E^0(D^+/D)$ of these dyes vary by up to 0.5 V.

For the series of Ruthenium bipyridyl dyes (**1**−**4**), the spatial separation of the dye cation state from the electrode surface was determined by semiempirical ZINDO/1 calculations as detailed above. Figure 1 shows the HOMO orbitals resulting from ZINDO/1 calculations performed on these complexes in their cation state. These data show a pseudooctahedral arrangement of ligands around the metal atom with different angles depending on the apical ligands, with the structural data (bond angles and distances) being in good agreement with previous studies by other groups of the charge neutral dyes (for example, our calculations yield Ru−N distances for the cation state of $Ru(dcbpy)_2(NCS)_2$ of 1.97 and 1.98 Å, similar to the distances of 2.036 and 2.058 Å reported previously for the neutral dye[35]). It is apparent from Figure 1 that for dye **1** the cation wave function is metal-localized, whereas for dye **4** the cation is

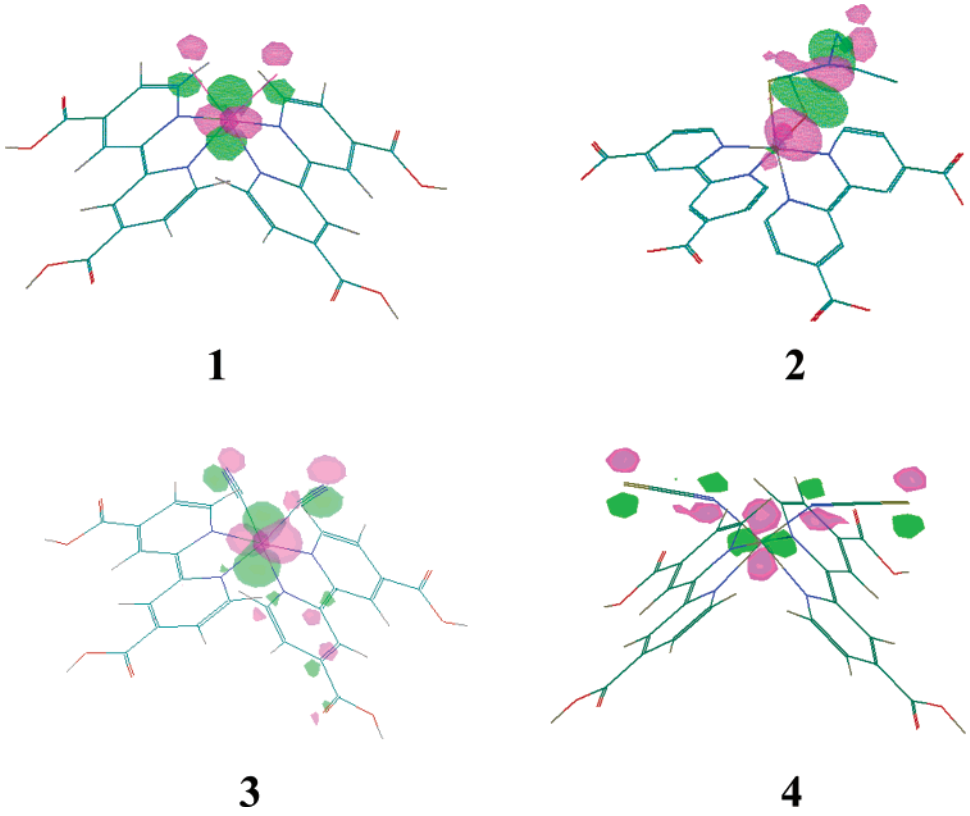

Figure 1. Graphical representation for the HOMO of $Ru(dcbpy)_2Cl_2$ (**1**), $Ru(dcbpy)_2DTC$ (**2**), $Ru(dcbpy)_2(CN)_2$ (**3**), and $Ru(dcbpy)_2(NCS)_2$ (**4**) cation states.

Table 1. Comparison of Electrochemical, Structural, and Recombination Kinetics Data for Nanocrystalline TiO_2 Films Sensitized by Dyes **1**−**8**

dye	$E^0(D^+/D)^a$/V	r^b/Å	$t_{50\%}{}^c$/ms	α^d
$Ru(dcbpy)_2Cl_2$ (**1**)	0.56	7.4	<0.06	0.11
$Ru(dcbpy)_2DTC$ (**2**)	0.8	8.3	0.11	0.21
$Ru(dcbpy)_2(CN)_2$ (**3**)	1	8.4	0.29	0.24
$Ru(dcbpy)_2(NCS)_2$ (**4**)	0.85	10.2	0.79	0.25
Zn−*meso*-porphyrin IX (**5**)	0.5		2.23	0.3
Zn−coproporphyrin 1 (**6**)	0.57		2.82	0.36
H_2TCPP (**7**)	1		4.38	0.33
$ZnPc(CH_2COOH)_4$ (**8**)	0.49		6.23	0.30

[a] Ground-state oxidation potentials determined from electrochemical data and shown versus SCE. [b] Spatial separation of the dye cation HOMO orbital from the electrode surface, detemined from semiempirical calculations. [c] $e^-_{TiO_2}/dye^+$ charge recombination half-time, determined from transient absorption studies. [d] Stretch parameter, α, as defined in eq 3, determined from numerical fits to the transient absorption data.

localized on the NCS ligands, consistent with previous calculations.[36] Dyes **2** and **3** lie intermediate between these two extremes.

The ZINDO/1 calculations provide us with the spatial distribution of the HOMO orbital of each dye, with the square of this distribution corresponding approximately to the dye cation electron density. All dyes in this series (dyes **1**−**4**) have the same structural components for achieving binding to the metal oxide surface (two dicarboxy bipyridyl groups) and are therefore expected to bind to the electrode surface with a similar orientation. The dye cation/TiO_2 electrode spatial separation was therefore estimated by calculating the geometric distance between the carboxylic groups and each atom of the dye and by weighting this value with the square of the percentage contribution of the atom to the HOMO orbital.[37] The resulting distances are also given in Table 1. It is apparent that ***r*** of the dye cation from the electrode surface is in the order **1** < **2** ∼ **3** < **4**, as is also apparent from the HOMO orbitals shown in Figure 1.

ZINDO/1 calculations were also performed on dyes **5**−**8**. In all cases the HOMO orbital was delocalized over the conjugated macrocycle of the dye. However, for these dyes, determination of a reliable donor/acceptor separation is prevented by uncertainty over the orientation of these molecules on the surface on TiO_2 as we discuss in more detail below.

Recombination dynamics for the dye-sensitized nanoporous TiO_2 films were determined by following the decay of the photoinduced absorption of the $e^-_{TiO_2}/dye^+$ state observed following photoinduced charge separation initiated by pulsed laser excitation of the film. Excitation densities were adjusted to ensure matched densities of absorbed photons for all sensitizer dyes, in all cases corresponding to ∼0.5 absorbed photons/TiO_2 particle. Photoinduced absorption changes were monitored at probe wavelengths between 600 and 900 nm. In the case of dye **4**, $Ru(dcbpy)_2(NCS)_2$ a strong absorption maximum was observed at 800 nm, assigned as discussed previously[33] to a LMCT transition resulting from the ligand-localized nature of the dye cation state. This absorption band is superimposed upon a relatively weak, broad $e^-_{TiO_2}$ absorption. For dyes **1**−**3**, no such cation band was observed, with only a relatively small

(36) Rensmo, H.; Lunell, S.; Siegbahn, H. J. *J. Photochem. Photobiol., A* **1998**, *114*, 117.

(37) The electronic coupling H_{AB} should correctly be determined by calculating the electronic coupling for each atom contributing to the dye HOMO orbital and then summing over all atoms. However, given the small spatial extent of the dye HOMO orbitals relative to their separation from the electrode surface, the method employed gives a good approximation to the variation in r and therefore H_{AB} between the different dyes.

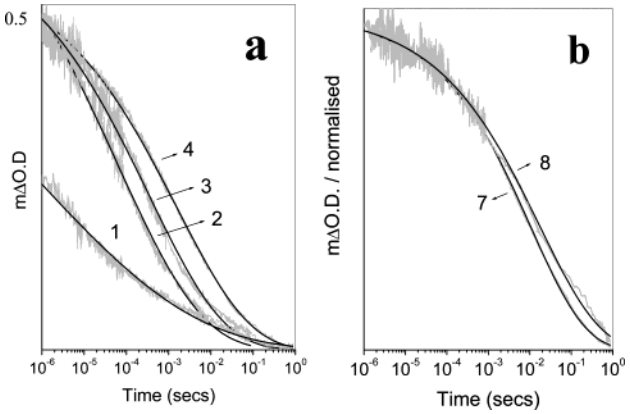

Figure 2. Transient absorption data monitoring the charge recombination kinetics for 8 μm TiO_2 films sensitized with (a) bipyridyl dyes **1** ($Ru(dcbpy)_2Cl_2$), **2** ($Ru(dcbpy)_2DTC$), **3** ($Ru(dcbpy)_2(CN)_2$), and **4** ($Ru(dcbpy)_2(NCS)_2$) and (b) the dyes **7** (H_2TCPP) and **8** ($ZnPc(CH_2COOH)_4$). Experiments employed excitation conditions resulting in matched densities of absorbed photons (see text for details). The solid lines are the fits to the stretched exponential function $\Delta OD \propto \exp(-(t/\tau)^{\alpha})$. For ease of comparison, the data for dye **4** is reduced in amplitude by a factor of 2.5, necessary due to the strong cation absorption for this dye at the probe wavelength (900 nm).

absorption being observed, increasing monotonically toward longer wavelengths. In accordance with previous observations, this is attributed to $e^-_{TiO_2}$ absorption. For dyes **5**−**8** the transient signal contained contributions from both the dye cation band and $e^-_{TiO_2}$ absorption. For all dyes, the decay dynamics of their red/near-infrared photoinduced absorption were found to be independent of the probe wavelength, except near isosbestic points of the transient spectra.

Typical transient absorption kinetics, assigned to charge recombination of $e^-_{TiO_2}$ with dye cation species, are shown in Figure 2, plotted on a logarithmic time scale. These experiments employed probe wavelengths of 900 nm for dyes **1**−**4**, 700 nm for dyes **5** and **7**, 750 nm for dye **6**, and 800 nm for dye **8**. It is apparent that the recombination dynamics vary in time scale by at least 2 orders of magnitude, depending upon the sensitizer dye employed. $t_{50\%}$ for the recombination dynamics for all sensitizer dyes determined from such data are shown in Table 1. For dye **1**, it is apparent that significant recombination probably occurs prior to instrument time resolution ($\sim$1 μs); the $t_{50\%}$ determined for this dye should therefore be regarded as a longer limit for the recombination time.

It is apparent from Figure 2 that the $e^-_{TiO_2}/dye^+$ recombination dynamics are dispersive, extending over a broad range of time scales for each dye. For all dyes, the transient absorption decay showed an excellent fit to a stretched exponential function (eq 3) as shown by the smooth gray lines in Figure 2.

$$\Delta OD(t) = \Delta OD_0 e^{-(t/\tau)\alpha} \qquad (3)$$

Values for α obtained from these numerical fits are also shown in Table 1, with low values of α corresponding to more dispersive kinetics.

It is apparent from Figure 2 that there is a clear correlation between the recombination half-time and the degree of dispersion of the kinetics, with the faster recombination dynamics being more dispersive. This correlation can be quantified by plotting the decay half-time against stretched exponential dispersion parameter α, as shown in Figure 3.

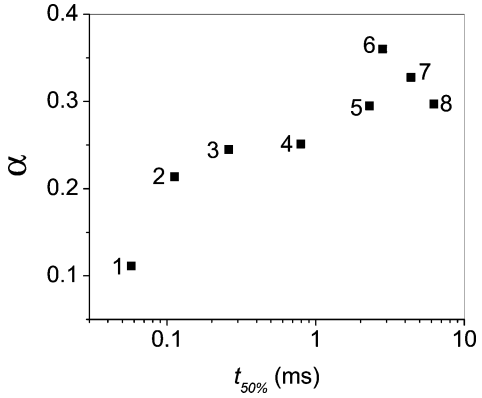

Figure 3. Plot of α, the stretched exponential dispersion parameter, versus the half-time $t_{50\%}$ for charge recombination for dyes **1**−**8,** determined from numerical fits of the transient absorption data shown in Figure 2 to eq 3.

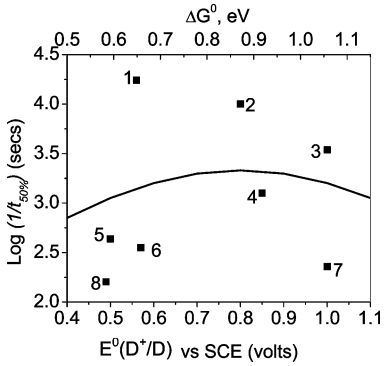

Figure 4. Plot of the logarithm of $1/t_{50\%}$ for charge recombination versus the ground-state oxidation potential of each dye $E^0(D^+/D)$ (lower *x*-axis) for nanocrystalline TiO_2 films sensitized by dyes **1**−**8**. The upper *x*-axis shows the corresponding estimated free energy driving force ΔG^0 for the charge recombination process. The smooth line shows the free energy dependence of $1/t_{50\%}$ expected from eq 1, assuming $k_{et} \propto 1/t_{50\%}$, with λ = 0.8 eV and constant H_{AB}.

Figures 4 and 5 address the correlation between the recombination $t_{50\%}$ and the reaction ΔG^0 (Figure 4) and between $t_{50\%}$ and the dye cation/electrode *r* (Figure 5). Figure 4 shows a plot of the logarithm of $1/t_{50\%}$ against the dye cation ground-state oxidation potential $E^0(D^+/D)$. The upper axis shows the corresponding ΔG^0 determined assuming a quasi-Fermi level within the TiO_2 electrode following laser excitation of −0.1 V vs SCE. The latter value was determined by comparison with recombination data collected under electrochemical bias control of the electrode Fermi level in a photoelectrochemical cell,[33] with the Fermi level rise induced by the laser excitation being determined to be $\sim$0.1 eV by transient photovoltage studies.[38] It is apparent from this figure that there is remarkably little correlation between the reaction half-time and free energy. For example, the reaction free energies for dyes **7** and **8** differ by 500 meV, yet their recombination half-times are essentially indistinguishable. Similarly, dyes **1**, **6**, and **8** have the same reaction free energies but exhibit recombination half-times varying by over 2 orders of magnitude.

Figure 5a addresses the correlation between the recombination half-time and spatial separation of the dye cation from the electrode surface determined from the ZINDO calculations. Due to the uncertainty over the orientation of dyes **5**−**9** on the electrode surface, data are only shown for dyes **1**−**4**. A clear

(38) Green, A.; Palomares, E. J.; Durrant, J. R. Manuscript in preparation.

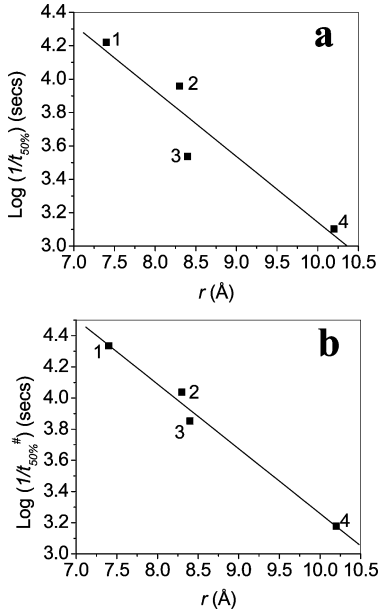

Figure 5. Plots of the logarithm of $1/t_{50\%}$ versus the spatial separation r of the dye cation from the TiO_2 surface for dyes **1**−**4** estimated from ZINDO/1 calculations: (a) direct comparison of the experimental $t_{50\%}$ data against r; (b) plot of free-energy-optimized $1/t_{50\%}^{\#}$, as defined in eq 4, against r. The straight lines are linear fits to the experimental data, following eq 2. From plot b we obtain a value for the slope of this line, β, of 0.95 ± 0.2 Å^{-1}.

linear correlation is apparent between the logarithm of the electron-transfer half-time and the spatial separation. Making the simple approximation that $k_{et} \propto 1/t_{50\%}$ (see Discussion below), it is apparent that this linear correlation is in good agreement with theoretical expectations, as detailed in eq 2.

Discussion

We have addressed the charge recombination dynamics of dye-sensitized, nanocrystalline TiO_2 films for a range of different sensitizer dyes. Charge recombination dynamics have been determined by transient laser spectroscopy, employing low-intensity excitation pulses, with the intensity adjusted to ensure equal densities of absorbed photons (~0.5 adsorbed photons per pulse per nanoparticle) for all sensitizer dyes. These dynamics have been correlated with differences in the ΔG^0 estimated from dye oxidation potentials determined from solution-phase electrochemistry and the r of the dye cation orbital from the electrode surface determined by semiempirical ZINDO/1 calculations.

***k_{et}* versus ΔG^0.** The data we present here show remarkably little correlation between the recombination dynamics and the reaction free energy. At first sight, this observation appears contrary to eq 1. This apparent contradiction can however be understood by quantitative consideration of the free energy dependence expected from eq 1. The variation in reaction half-time predicted by eq 1, assuming $\lambda = 0.8$ eV,[39] is therefore shown as the smooth line in Figure 4. It is apparent that over the range of reaction free energies considered in this study, eq 1 predicts only a modest dependence of reaction half-time upon ΔG^0. This modest dependence can be readily understood in terms of the relatively large value of λ, with all the data lying in the range of $\Delta G^0 \sim \lambda$, where the dependence of k_{et} upon ΔG^0 is expected to be minimal.

The recombination data we report here do not lie significantly in the Marcus inverted region ($\Delta G^0 > \lambda$), and indeed lie closer to $\Delta G^0 \sim \lambda$. We note that ΔG^0 depends on both the dye oxidation potential and the Fermi level of the metal oxide film. Under the conditions of our experiment, we estimate an effective TiO_2 Fermi level following laser excitation of −0.1 V vs SCE. Under device operating conditions, the Fermi level is expected to be in the range of −0.3 to −0.6 V vs SCE (i.e., cell voltages versus I^-/I_2 of 0.5 to 0.8 V), resulting in a 0.2 to 0.5 V increase in ΔG^0 compared to the experimental conditions employed here. Depending upon the dye employed, such an increase will result in a modest shift of the reaction into the Marcus inverted region and therefore an increase in the dependence of the recombination dynamics upon $E^0(D^+/D)$.

We note that the free energy analysis discussed above does not take into consideration integration of eq 1 over all occupied electronic states of the electrode. The TiO_2 electrodes employed in this study exhibit an exponential density of states extending into the material band gap ($g(E) = N/kT_0 \exp(-(E_{cb} - E)/k_BT_0)$), with injected electrons occupying this density of states up to the effective quasi-Fermi level. Previous studies have yielded values for k_BT_0 in the range 60−200 meV.[40] Due to this exponential density of states, and the low density of photoinjected electrons employed in the studies reported here, the majority of injected electrons will occupy states with energies close to the quasi-Fermi level; under such conditions calculation of k_{et} using eq 1 with a single value for $\Delta G^0 = E_F - E^0(D/D^+)$, and using eq 1 including integration over all occupied donor states of the electrode yielded rather similar results. Integration over all occupied donor states in fact resulted in a reduced dependence of k_{et} upon $E^0(D/D^+)$, further emphasizing the weak dependence of the recombination dynamics upon dye oxidation potential.

***k_{et}* versus *r*.** Figure 5a shows a direct comparison between the experimentally determined $t_{50\%}$ and r. The approximately linear behavior observed in this figure is in agreement with theoretical expectations for electron tunneling, as expressed in eqs 1 and 2. It can therefore be concluded that r is a key parameter in determining the kinetics of charge recombination.

Figure 5b provides a more precise analysis of the distance dependence of the charge recombination dynamics, in which the ΔG^0 dependence of the dynamics, as predicted from eq 1, is also factored into the data by using

$$t_{50\%}^{\#} = t_{50\%} \exp\left(\frac{(\Delta G^0 - \lambda)^2}{4\lambda k_B T}\right) \qquad (4)$$

where the exponential term in this equation corresponds to the retardation of the recombination dynamics expected for each dye as the reaction free energy moves away from the ideal (activationless, $\Delta G^0 = \lambda$) case. The plot of $\log(1/t_{50\%}^{\#})$ versus r therefore allows a direct analysis of the distance dependence

(39) Previous studies have reported values of λ in the range of 1−1.4 eV.[20−23] These values have however been obtained with the assumption that the electrode Fermi level can be equated with reported conduction band edge for the bulk metal oxide. Our own studies have included studies in which the Fermi level of the nanocrystalline film is controlled directly by an application of applied potential in a three-electrode photoelectrochemical cell.[40] These studies suggest that the value of E_F assumed in the studies by other groups may be too negative, resulting in an overestimate of λ. Taking into account these considerations, we therefore assume a value for λ of 0.8 V.

(40) Willis, R. L.; Olson, C.; O'Regan, B.; Lutz, T.; Nelson, J.; Durrant, J. R. *J. Phys. Chem. B* **2002**, *106*, 7605−7613.

of the reaction dynamics alone. A linear behavior is again observed, in agreement with eq 2. It is furthermore apparent that the fit to this linear behavior is significantly better when employing the free-energy-optimized $t_{50\%}^{\#}$ (Figure 5b) compared to that employing the unoptimized data $t_{50\%}$ (Figure 5a), consistent with the reaction dynamics, indeed following the ΔG^0 dependence given by eqs 1 and 4. However, we emphasize that the improvement in the fit to linear behavior is marginal, indicating that the primary factor influencing the reaction rate is r, with ΔG^0 being of only secondary importance. We note that a similar conclusion has also been reached for biological electron-transfer dynamics, where extensive studies have demonstrated that the primary factor influencing the rate constants for electron transfer between redox sites in proteins is their spatial separation, with the reaction free energy again being of only secondary importance.[5]

Evaluation of the gradient of the straight-line fit in Figure 5b allows determination of β, indicative of the barrier height to electron tunneling. From this linear fit to the data, we obtain a value for β of 0.95 ± 0.2 Å^{-1}. This value of β is in good agreement with previous studies of through-bond electron coupling for both homogeneous and interfacial electron transfer.[5,18,41] This observation clearly demonstrates the importance of spatial separation in controlling the interfacial recombination dynamics and provides a quantitative ruler for this dependence. We note that such a quantitative relationship has not been, to our knowledge, reported previously for this experimental system, with the only previously detailed study of this dependence reporting distance-independent recombination dynamics.[24] This distance dependence is however in agreement with electrochemical studies of interfacial electron-transfer dynamics between flat electrode surfaces and redox molecules adsorbed as self-assembled monolayers as a function of spacer separation.[42]

Dyes **5**−**8**, comprising porphyrins and a phthalocyanine, all exhibited slower recombination dynamics compared to the ruthenium bipyridyl dyes **1**−**4**. Dyes **5**−**8** are all bound to the electrode surface through peripheral carboxylate ligands with the dye cation orbital delocalized over the conjugated macrocycle (as determined from semiempirical ZINDO/1 calculations), consistent with relatively weak electronic coupling H_{AB}^2 being the origin of the slower recombination dynamics. However, uncertainty over the orientation of these dyes on the metal oxide surface prevents quantitative analysis of this behavior.

The strong distance dependence reported here has significant implications for the design of sensitizer dyes for dye-sensitized solar cells. It suggests that small, strongly bound sensitizer dyes, while favoring ultrafast electron injection, will also exhibit rapid recombination dynamics, which may ultimately limit device performance.[25]

***k*$_{et}$ versus α.** Figure 3 shows a clear correlation between the recombination half time and the degree of dispersion of the kinetics, as defined by the stretched exponential dispersion parameter α defined by eq 3. It is apparent that as the recombination half-time is reduced, the dynamics become increasingly dispersive (small α). This observation is consistent with our previously reported comparison of recombination dynamics for two free base porphyrins.[19] The addition of triphenylamine groups to the periphery of the porphyrin macrocycle was observed to result in 20-fold retardation of the recombination dynamics, assigned to an increased spatial separation of the dye cation from the metal oxide surface. Concomitant with this retardation, the recombination dynamics shifted from stretched exponential behavior ($\alpha = 0.31$) to a monoexponential decay. This transition was assigned to a shift from electron-transport-limited recombination in the limit of strong electronic coupling to interfacial electron-transfer-limited recombination in the limit of low electronic coupling, as illustrated in Scheme 1. Following this analysis, the correlation between $t_{50\%}$ and α shown in Figure 3 can be attributed to a shift from more transport-limited recombination (for faster, more dispersive recombination dynamics) to more interfacial electron-transfer-limited dynamics (for slower, less dispersive dynamics).

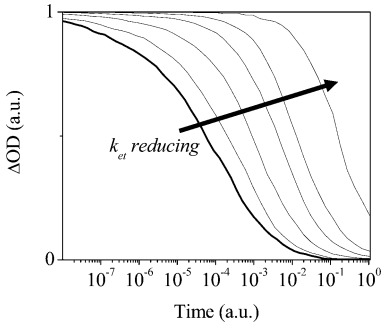

Figure 6. Model calculations for the dependence of the charge recombination dynamics upon a 1000-fold reduction in the electron-transfer rate constant k_{et}. Calculations based on the CTRW model, with the addition of kinetic competition for electrons in the reactive sites between recombination with the dye cation (with a rate constant k_{et}) and thermally activated detrapping and transfer to an adjacent trap site.

Monte Carlo simulations of the recombination dynamics were conducted to allow a more quantitative analysis of this model. Calculations were based upon the continuous-time random walk model we have reported previously, corresponding to electron transport in the TiO_2 film being controlled by thermally activated detrapping from an exponential distribution of trap sites. Our previous calculations have assumed that charge recombination occurs once the electron reaches a reactive site (i.e., a site adjacent to a dye cation). The calculations reported here are distinct in that they include a branching for electrons in the reactive sites between recombination with the dye cation (with a probability P_{et} proportional to the rate constant k_{et}) and thermally activated detrapping and transfer to an adjacent trap site.

The effect of k_{et}, on recombination dynamics, was simulated using the Monte Carlo model modified as explained above. The model system was similar to that used previously by Nelson et al.,[27] consisting of a spherical shell of radius 17 and thickness 3 lattice units, representing a TiO_2 nanoparticle of 15 nm diameter. The room-temperature density of states parameter γ was 0.3, and simulations were carried out with 1 dye cation and 3 electrons, allowing for dark conduction electrons in the film. P_{et} was varied between 1, representing prompt recombination, and 0.001. Simulated kinetic curves are presented in Figure 6. It is clear that the curve evolves from a stretched exponential of dispersion parameter $\alpha = 0.3$ toward more monoexponential behavior as P_{et} is reduced. In the limit of $P_{et} = 1$ ($k_{et} \rightarrow \infty$), the recombination dynamics are limited by the first passage time to the reactive sites, resulting in dispersive recombination

(41) Miller, R. J. D.; McLendon, G. L.; Nozik, A. J.; Schmickler, W.; Willig, F. *Surface Electron Transfer Processes*; VCH: New York, 1995.
(42) Miller, C.; Cuendet, P.; Gratzel, M. *J. Phys. Chem.* **1991**, *95*, 877.

dynamics as we have reported previously. In the limit of $P_{et} \rightarrow 0$ (slow k_{et}), electrons must visit the reactive site many times before recombination occurs, resulting in a more monoexponential decay. The value of k_{et} at which the process becomes monoexponential depends on the time needed for the electron to freely explore the film and will be longer for deeper distributions of trap states.

A rigorous comparison of this theoretical model with experimental observations would require the collection of experimental data for each dye under conditions of electrochemically applied external bias. Such studies are beyond the scope of this paper. Nevertheless, the model calculation results shown in Figure 6 are in good qualitative agreement with the experimentally observed shift between fast, dispersive dynamics to slower, less dispersive dynamics observed for different sensitizer dyes, consistent with a transition from electron transport limited to interfacial electron-transfer-limited dynamics.

We have assumed above that the electron-transfer rate constant is related to the experimentally observed reaction half-time by $k_{et} \propto 1/t_{50\%}$. This assumption needs to be qualified in two respects. First, $t_{50\%}$ is dependent on not only the interfacial k_{et} but also the electron transport dynamics with TiO_2. In the simulations we have restricted explicit attention to cases where k_{et} is no faster than the attempt-to-jump frequency for charge transport. Typically that means restricting k_{et} to less than 10^{11} or 10^{12} s^{-1}, which is well-justified by observation. Faster values of k_{et} would result in a regime where the kinetics are identical to the case of $P_{et} = 1$ and are limited only by charge transport. However, there is no evidence that this regime is relevant for the systems studied here, so it is not considered. Second, it would appear that a small change in the probability of recombination once an electron reaches a reactive site should result in the same relative change in the net recombination kinetics, yet simulations show that the dependence on P_{et}^{-1} is slightly stronger, such that $t_{50\%} \propto k_{et}^{-1.2}$ (see Supporting Information). This deviation from proportionality is due to the variation in the dispersion parameter α. However, the deviation is sufficiently small, as we discuss in the Supporting Information, that our assumption of $k_{et} \propto 1/t_{50\%}$ is indeed a reasonable approximation, allowing us to relate our experimental observations to the electron-transfer rate constant.

Implications for Device Optimization. The development of sensitizer dyes for dye-sensitized photovoltaic cells requires consideration of a range of distinct, and often conflicting, constraints. One of these constraints is the minimization of interfacial recombination dynamics. We have considered two possible means by which to control these interfacial dynamics, namely, the dye oxidation potential $E^0(D^+/D)$ and the spatial separation of the dye cation from the electrode surface. We find the recombination dynamics are only weakly dependent upon $E^0(D^+/D)$. Given that the ability to modulate $E^0(D^+/D)$ is in addition constrained by the need to achieve favorable energetics for the electron injection and dye cation regeneration reactions, we conclude that the recombination dynamics cannot be usefully modulated by variation of $E^0(D^+/D)$. In contrast we find that variation of the spatial separation of the dye cation from electrode surface results in significant variations in recombination dynamics and is indeed an attractive route to modulating these dynamics.

$Ru(dcbpy)_2(NCS)_2$ (dye **4**) is widely acknowledged as one of the most promising sensitizer dyes reported to date. Comparing this dye with a series of structurally analogous ruthenium bipyridyl dyes, we indeed find this dye exhibits the slowest recombination dynamics of this series. Recombination dynamics for this dye lie in the intermediate regime between electron-transport-limited and interfacial electron-transfer-limited recombination and can be expected to be sensitive to both the electron mobility with the TiO_2 film and the interfacial electron-transfer rate constant. The slow recombination dynamics for this dye do not result primarily from the reaction free energy lying in the Marcus inverted region. Rather these slower dynamics result from an increased spatial separation of the dye cation from the electrode surface.

Acknowledgment. We gratefully acknowledge the financial support from EPRSC, the Swiss Federal Office for Energy (OFEN), and the U.S. Air Force Research Office under Contract No. F61775-00-C0003. E.P. is very grateful for the support of a Marie Curie Fellowship (HPMF-CT-2002-01744). Supply of the N719 dye from Johnson Matthey Ltd. is also gratefully acknowledged.

Supporting Information Available: Experimental plot (PDF). This material is available free of charge via the Internet at http://pubs.acs.org.

JA039924N